



Numerical simulation-based performance improvement of the separation of circulating tumor cells from bloodstream in a microfluidic platform by dielectrophoresis

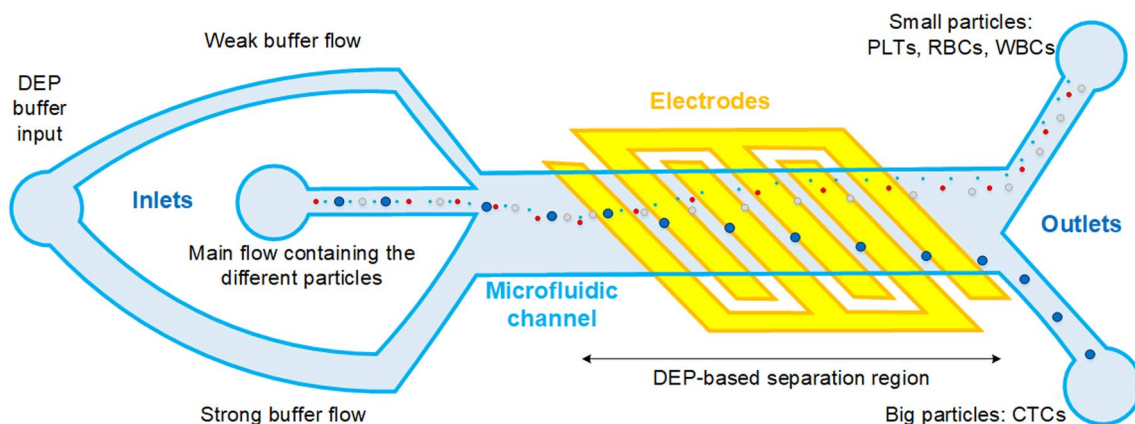
Ngoc-Viet Nguyen^{1,2} · Hoang Van Manh³ · Nguyen Van Hieu^{1,2}

Received: 23 January 2022 / Revised: 22 July 2022 / Accepted: 31 July 2022 / Published online: 12 August 2022
© Korean Society of Rheology 2022

Abstract

Circulating tumor cells (CTCs) detection has become one of the promising solutions for the early diagnosis of cancers. Thus, the separation of CTCs is of great importance in biomedical applications. In addition, microfluidic technology has been an attractive approach to the manipulation of biological cells. This study presents the parametric investigations relevant to the volumetric throughput of a microfluidic platform with the dielectrophoresis (DEP)-based cell manipulation technique for the continuous CTCs separation. A low potential voltage at an appropriate frequency was applied to slanted planar electrodes to separate CTCs from normal cells in blood samples due to mainly the cell size difference. The performance of the separation process was analyzed by evaluating the cell trajectories, purity, and recovery rates. Several inlet flow rates of buffer and cell sample fluid streams were examined. Various channel configurations with different outlet and height dimensions were also investigated to enhance the isolation of CTCs. During the simulation, the size and shape of cells were assumed as fixed-sized, solid spheres. The results showed that CTCs could be separated from blood cells, including white blood cells (WBCs), red blood cells (RBCs), and platelets (PLTs) with recovery and purity factors up to 100% at the cell sample throughput of 10 $\mu\text{L}/\text{min}$ by utilizing a suitable microchannel design. The current study significantly contributes valuable insights into the design of the microchip devices to effectively and selectively isolate different cancerous cells in biofluids.

Graphical abstract



Keywords Circulating tumor cell · Continuous cell separation · Dielectrophoresis microfluidic chip · Numerical simulation · Flow rate

✉ Ngoc-Viet Nguyen
viet.nguyenngoc@phenikaa-uni.edu.vn

Extended author information available on the last page of the article

1 Introduction

Cancer is the first or second leading death cause in worldwide human diseases, with over 19 million new cases and about 10 million deaths each year [46]. The two most common cancer types are breast cancer in women and lung cancer in men. Early detection methods of these cancer diseases and related research issues have received a lot of attention [9, 14, 17, 50]. The progression in each kind of cancer is frequently expressed at different cytological levels by the cell molecular, morphology, and proliferation difference. A standard blood sample consists of various typical components, such as white blood cells (WBCs), red blood cells (RBCs), and platelets (PLTs). In some cancer patient cases, various specific cell lines also appear in the peripheral bloodstream, or the blood circulation system, in particular rare cell types with a low appearance in the sample less than 10^3 cells/mL, such as stem cells, circulating fetal cells, and circulating tumor cells (CTCs) [10, 42]. Isolation, identification, and characterization of those rare cells are indispensable for a wide range of biomedical applications. It is potential for doctors to choose appropriate and effective treatment methods. CTCs are considered prognostic biomarkers relevant to the primary and even metastatic tumors [30]. In reality, CTCs are sparse in the peripheral blood (below 10^2 cells per 10^9 hematologic cells) and their heterogeneous and fragile features [43]. Collection and enrichment methods can raise CTCs accumulation, thereby enhancing detection efficacy and accuracy, as well as, providing a reliable diagnosis for cancer treatment. A robust device would have high CTCs purity and recovery rates, high throughput, and clinical relevance.

Microfluidic-based approaches combining electric, acoustic, magnetic, or optical techniques have emerged as a powerful solution for the purification of microparticles [9, 20, 25, 29]. The separation of specific particles in microfluidic platforms has been critical in biomedical applications [3, 8, 16, 18, 29, 44, 49, 51]. Up to now, a series of researches on the use of microfluidic technologies have been reported to focus cellular components [45]. A variety of microfluidic devices have been improved for the manipulation of cancer cells, including CTCs [2, 14, 37, 48]. The main benefits are low complexity, simplicity to fabricate, and good compatibility with the miniaturized systems. Almost all these microchips often contain a two-step procedure of cell isolation and subsequent cell detection. Hence, the development of particular devices for separating CTCs from whole blood specimens is a crucial demand for successful subsequent analysis and detection applications. Electric principles have gained much attention due to their advantages, such as simplicity, easy

operation, rapid processing time, and low cost [9, 10, 38]. Dielectrophoresis (DEP) that exerts forces on dielectric particles suspended in a non-uniform electric field, has emerged as a rapid, label-free, and cell-friendly approach for manipulating cells [11, 20, 28, 42, 47]. The potency of the DEP method heavily relies on the dimension and electrical properties of the cell particle, the conductivity and permittivity of the flow medium, and the magnitude and frequency of the applied electric field. The Clausius–Mosotti (CM) factor is used to classify DEP response into positive DEP (pDEP) if the real part of the CM factor is greater than 0 and negative DEP (nDEP) if this one is less than 0 [33]. Then, cells forced by pDEP are guided toward the high electric field strength location, whereas cells forced by nDEP are moved to the low electric gradients. A large number of DEP-based microchips have been developed for cancer cell capture and detection applications. Cell size-based enrichment features and DEP-based microfluidic methods are prominent in CTCs isolation [6, 22]. The efficiency of the separation process frequently increased with decreasing sample flow rate or rising applied voltage. The separation performance of the DEP microfluidic devices was typically found to be approximately 90% at the optimal fluid flow rates introduced to the channel below $1.0 \mu\text{L}/\text{min}$. In some prototypes, the flow rate could reach up to $1.5 \mu\text{L}/\text{min}$, but the excitation voltage amplitude was operated to hundreds of volts [27, 31]. In general, a few drawbacks of the microchips still exist regarding low throughputs. Thus, improving the design and actuation parameters to strengthen the cell throughput is critical in DEP-combined microfluidic devices [7].

In recent years, the rapid advance of computational tools has allowed numerical simulations of continuous separation of micro-objects in models at the scale of practical experimental microfluidic devices. The finite element methods (FEMs) were used to explain the phenomena, estimate microparticle manipulation systems, or optimize their performances. Modeling and simulation methods have been continued to be chosen as versatile tools for many cell manipulation applications in microfluidics. Several mathematical models of DEP cell separators with high precision were found in the literature [5, 15, 24, 49]. Microchannel and electrode designs, fluidic flow and electric excitations, and cell features were commonly analyzed to improve separation performances. Blood cell sorting operations (RBCs, WBCs, and PLTs) in DEP-based microchips were significantly demonstrated through computational analyses [4, 19, 26, 32, 41]. Numerical studies of the DEP method were also successfully applied for the isolation of CTCs [1, 12, 35]. Very recently, a DEP-based microfluidic separator using slanted coplanar interdigitated electrodes has been studied towards the applications of cell manipulation [13]. The effects of various geometrical and operational parameters on

the DEP-induced displacement of particles were examined, including the width and deflection angle of the electrodes, the width and length of the channel, the particle size, and the total volumetric throughput. In the current work, the microfluidic platform is further modified to apply for separating CTCs from the bloodstream. Numerical simulations of the cell trajectories in the microchannel are presented. Investigations on the cell sample and buffer flow rates, different channel outlet and height models are carried out to find the highest separation efficiency. The obtained results indicate that the developed microfluidic chip is reliable for isolating and detecting tumor cells.

2 Materials and methods

2.1 Theoretical background

Ohm’s law, Gauss’s law, and continuity equations for the current are used to model the electric field in the microfluidic chip, as follows:

$$\vec{J} = \sigma \vec{E} + j\omega \vec{D} + \vec{J}_e \tag{1}$$

$$\nabla \cdot \vec{J} = 0 \tag{2}$$

$$\vec{E} = -\nabla \vec{V} \tag{3}$$

$$\vec{D} = \epsilon_0 \epsilon_m \vec{E} \tag{4}$$

where \vec{J} is the current density (A/m²), σ is the electrical conductivity (S/m), $\epsilon_0 = 8.85 \times 10^{-12}$ (F/m) is the vacuum permittivity, ϵ_m is the relative permittivity of the medium, \vec{E} is the electric field (V/m), ω is the angular frequency (rad/s), \vec{D} is the electric displacement field (C/m²), \vec{J}_e is the externally generated current density (A/m²), q is the space charge density (C/m²), and \vec{V} is the electric potential (V).

To solve the fluid flow velocity field, the Navier–Stokes continuity and momentum equations for the incompressible fluid motion in the microchannel are given by

$$\rho \nabla \cdot \vec{u}_m = 0 \tag{5}$$

$$\rho \left(\frac{\partial \vec{u}_m}{\partial t} + \vec{u}_m \cdot \nabla \vec{u}_m \right) = -\nabla p + \eta \nabla \cdot \left[\nabla \vec{u}_m + (\nabla \vec{u}_m)^T \right] \tag{6}$$

where \vec{u}_m is the fluid velocity vector (m/s), t is time, p is the pressure (Pa), ρ is the fluid density (kg/m³), and η is the fluid dynamic viscosity (Pa.s).

In the streamlines of the fluidic flow and the non-uniform electric field around the electrodes, the movement of a cell particle in the microchannel is mainly impacted by the DEP force

(\vec{F}_{DEP}), and the Stoke’s drag force (\vec{F}_{HD}). The cell motion can be expressed by Newton’s second law:

$$\vec{F}_{DEP} + \vec{F}_{HD} = m_p \frac{d\vec{u}_p}{dt} \tag{7}$$

where \vec{u}_p and m_p are the velocity and mass of the cell, respectively.

The DEP force \vec{F}_{DEP} inducing on a particle with the spherical shape of d_p diameter, in a suspension medium with the relative permittivity ϵ_m is described by

$$\vec{F}_{DEP} = \frac{1}{4} \pi d_p^3 \epsilon_0 \epsilon_m \text{Re}(f_{CM}) \nabla |E_{rms}|^2 \tag{8}$$

where E_{rms} is the root mean square of the electric field. $\text{Re}(f_{CM})$ is the real part of the Clausius–Mossotti (CM) factor and given by

$$f_{CM} = \frac{\epsilon_p^* - \epsilon_m^*}{\epsilon_p^* + 2\epsilon_m^*} \tag{9}$$

with the subscripts, p and m are the represented characters of the particle and the medium, respectively. The ϵ_i^* is the complex electrical permittivity, and expressed as

$$\epsilon_i^* = \epsilon_i - j \frac{\sigma_i}{\omega}; i = p, m \tag{10}$$

where σ is the electrical conductivity, ϵ is the permittivity, j is the imaginary unit and ω is the angular frequency of the electric field.

The CM factor of viable cells can be given by [23]

$$f_{CM}(\omega) = -\frac{\omega^2 (\tau_m \tau_p^* - \tau_p \tau_m^*) + j\omega (\tau_m^* - \tau_m - \tau_p^*) - 1}{\omega^2 (2\tau_m \tau_p^* - \tau_p \tau_m^*) - j\omega (\tau_m^* + 2\tau_m - \tau_p^*) - 2} \tag{11}$$

where $\tau_m^* = c_m r_p / \sigma_m$, $\tau_m = \epsilon_0 \epsilon_m / \sigma_m$, $\tau_p^* = c_m r_p / \sigma_p$, and $\tau_p = \epsilon_0 \epsilon_p / \sigma_p$ are time constants of the suspension medium, and the cell, separately. c_m is the cell membrane capacitance. Therefore, the DEP force acting on a cell is dependent upon the cell size, the electric factors of cell and media, and the applied electric field. A DEP factor can be defined by the formula:

$$\text{DEP factor} = \frac{1}{4} \pi d_p^3 \epsilon_0 \epsilon_m \text{Re}(f_{CM}) \tag{12}$$

Flow in the microfluidic channel can be freely considered as creeping flow and the Reynolds number is too small ($\text{Re} < 1$). Therefore, the hydrodynamic drag force \vec{F}_{HD} for a cell particle can be defined by Stokes’s law:

$$\vec{F}_{HD} = 3\pi \eta d_p (\vec{u}_m - \vec{u}_p) \tag{13}$$

where \vec{u}_m and \vec{u}_p are velocities of fluid and particle, respectively.

2.2 Microfluidic chip design

The proposed microfluidic platform for the continuous flow separation of biological particles based on the impact of hydrodynamic drag and lateral nDEP forces is depicted in Fig. 1. The primary slices of the microchip include an array of slanted planar microelectrodes and a straight channel structure layer [13]. The polydimethylsiloxane (PDMS) channel and gold electrode configuration patterned on the glass substrate can be fabricated using a similar soft lithography process in the laboratory [33, 34, 36]. These bio-compatible materials have been used extensively in assays for manipulation of cells. The microfluidic inlets contain DEP buffer and cell sample infusions. The main flow (different cell particles dispersed in DEP buffer) is injected into the In2 port, while the two DEP buffer flows are pumped into the In1 and In3 ports, respectively. The width of the In1 port is smaller than one of the In3 port to generate the weak and robust streams on either side of the main sample flow. With this sheath-assisted focusing mechanism [40], all the cell particles are focused in a limited breadth towards the main channel. Subsequently, the cells enter the DEP region, where the interdigitated microelectrodes are located. The electrodes employing AC non-uniform electric field are driven to sort and separate cells continuously. The two other outlet ports of Out1 and Out2 are the cell enrichment exits of the separation part. The width ratio between these two outlet ports can be modified to create different flow rates moving through the outlets. All the cells are manipulated by nDEP at a low applied voltage and a proper frequency. Under suitable conditions, the big particles are repelled to go out at the Out2, while the small particles are collected at the Out1. Because of the major distinction in the size of

cell types, there are high differences in the forces between cancerous and blood cells. The trajectories of various cell types and the forces acting on cells when they move passing over the interdigitated electrodes area are also illustrated in Fig. 1. Cancer cells or CTCs with large diameters have a big lateral displacement, end down in the separation region, and flow into Out2. The lateral displacement of smaller cells is somewhat reduced in the separation region, and normal cells are thus flow into Out1. As a result, the larger CTCs could be well separated from the smaller blood cells [19, 21]. The microfluidic platform can also be used to achieve continuous separation of cells based on their size [22].

2.3 Simulation parameters and setup

Three-dimensional (3D) geometrical parameters of the platform are given in Table 1. COMSOL Multiphysics (Ver5.2) was used in this study to perform numerical simulations of

Table 1 Initial parameters for the simulation model of DEP-based cell separation in the microfluidic chip [13]

Parameters	Symbol	Value
Height of the microchannel (μm)	H	40
Length of the main straight channel (μm)	L	14,000
Width of the main straight channel (μm)	W	800
Width of the Inlet 1 (μm)	$In1$	100
Width of the Inlet 2 (μm)	$In2$	300
Width of the Inlet 3 (μm)	$In3$	400
Width of the Outlet 1 (μm)	$Out1$	400
Width of the Outlet 2 (μm)	$Out2$	400
Width of the electrodes (μm)	we	60
Space between the two adjacent electrodes (μm)	se	20
Angle between the electrodes and the straight channel ($^\circ$)	θ	10

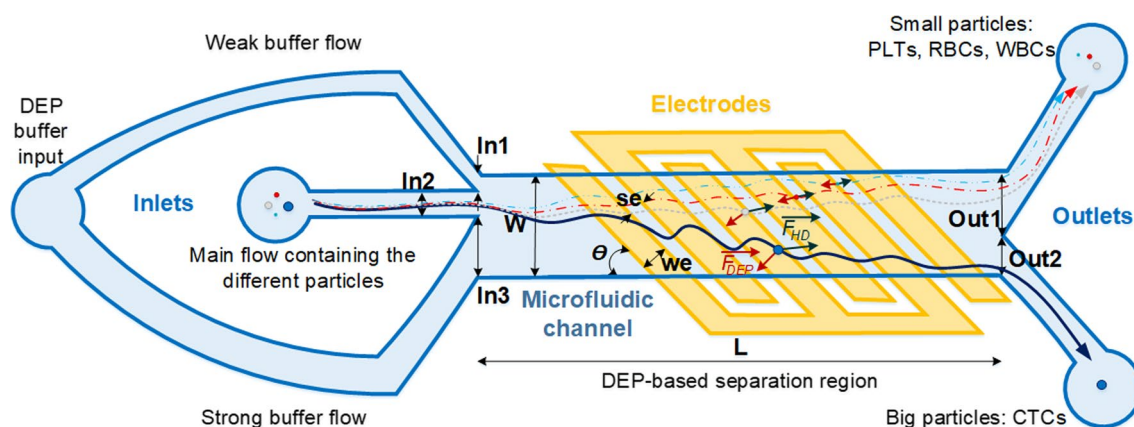


Fig. 1 Sketch the microfluidic channel with slanted planar microelectrodes for continuous particle separation based on hydrodynamic fluid flow and DEP forces

Table 2 Simulated size and electric parameters of cells: PLTs, RBCs, WBCs [4], and CTCs [47]

Properties	PLT	RBC	WBC	CTC (A549)
Particle diameter (μm)	2	7	12	17
Cytoplasm conductivity (S/m)	0.25	0.31	0.65	0.78
Cytoplasm relative permittivity (ϵ_0)	50	59	60	52
Membrane conductivity ($\mu\text{S/m}$)	1.0	1.0	27.4	25
Membrane relative permittivity (ϵ_0)	6.8	4.44	6	11.75
Membrane capacitance ($\mu\text{F/cm}^2$)	0.5	0.9	1.5	2.1
Membrane thickness (μm)	0.008	0.009	0.007	0.015

the continuous flow separation of cells. A549 lung CTCs [47], and PLTs, RBCs, WBCs [4] were chosen as simulated objects. In studying the motion trace of particles, cells could be simplified as spheres [39]. All cells were thus assumed

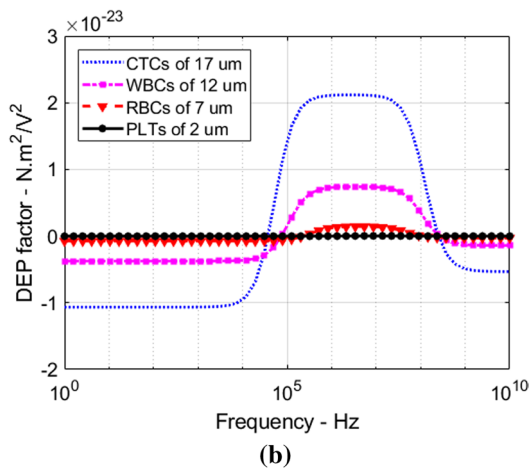
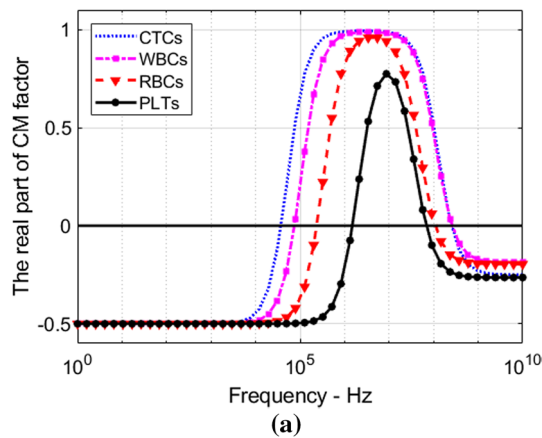


Fig. 2 a Calculated Clausius–Mossotti factors for different cell particles within the frequency range. The relative dielectric permittivity coefficient and the conductivity of the DEP medium are 78 and 0.055 S/m, respectively. **b** DEP force factors for cell types within the frequency range

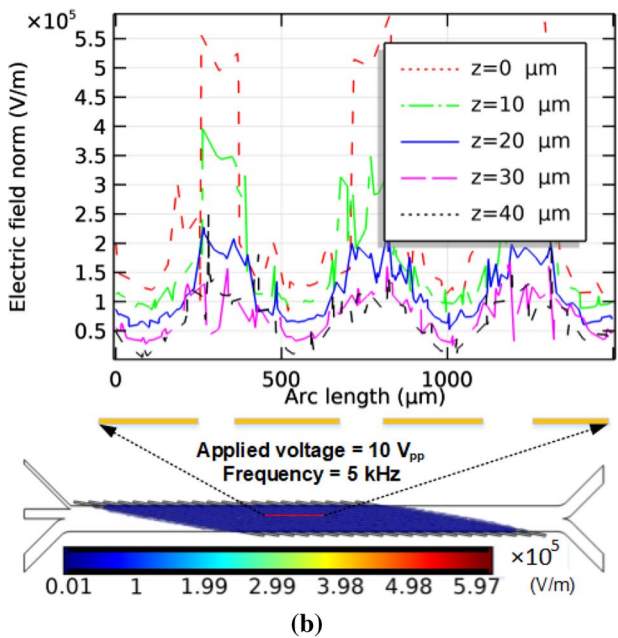
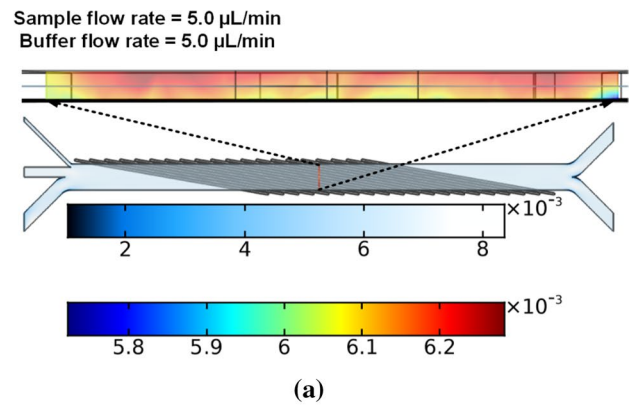


Fig. 3 a Distribution of the velocity field in the central cross sections of the channel, with the total fluid flow rate of 10 $\mu\text{L/min}$. **b** Simulated contours of the electric field magnitude around the microelectrodes in the sucrose medium. The voltage applied to the electrode pair is 10 V_{pp} , at the frequency of 5 kHz. Electric field profile across the section A–A’ at different heights, z , from the bottom surface of the electrodes patterned on the substrate

as spherical particles with the single-shell dielectric model, including a cytoplasm surrounded by a thin lipid membrane layer. The sizes and electrical properties of these types of cells were found in the literature and given in Table 2. In this study, we aim to isolate CTCs from other blood cells using nDEP manipulation. The DEP medium could be phosphate buffer saline (PBS) diluted in sucrose solution (its density and viscosity as the same as water: $\rho = 1.0 \times 10^3 \text{ kg/m}^3$, $\mu = 1.0 \times 10^{-3} \text{ N.s/m}^2$), with the relative permittivity about 78, and the conductivity of 0.055 S/m [35]. Figure 2a shows the real part graphs of CM factors calculated by Eq. (11) as functions of frequency for four kinds of cells.

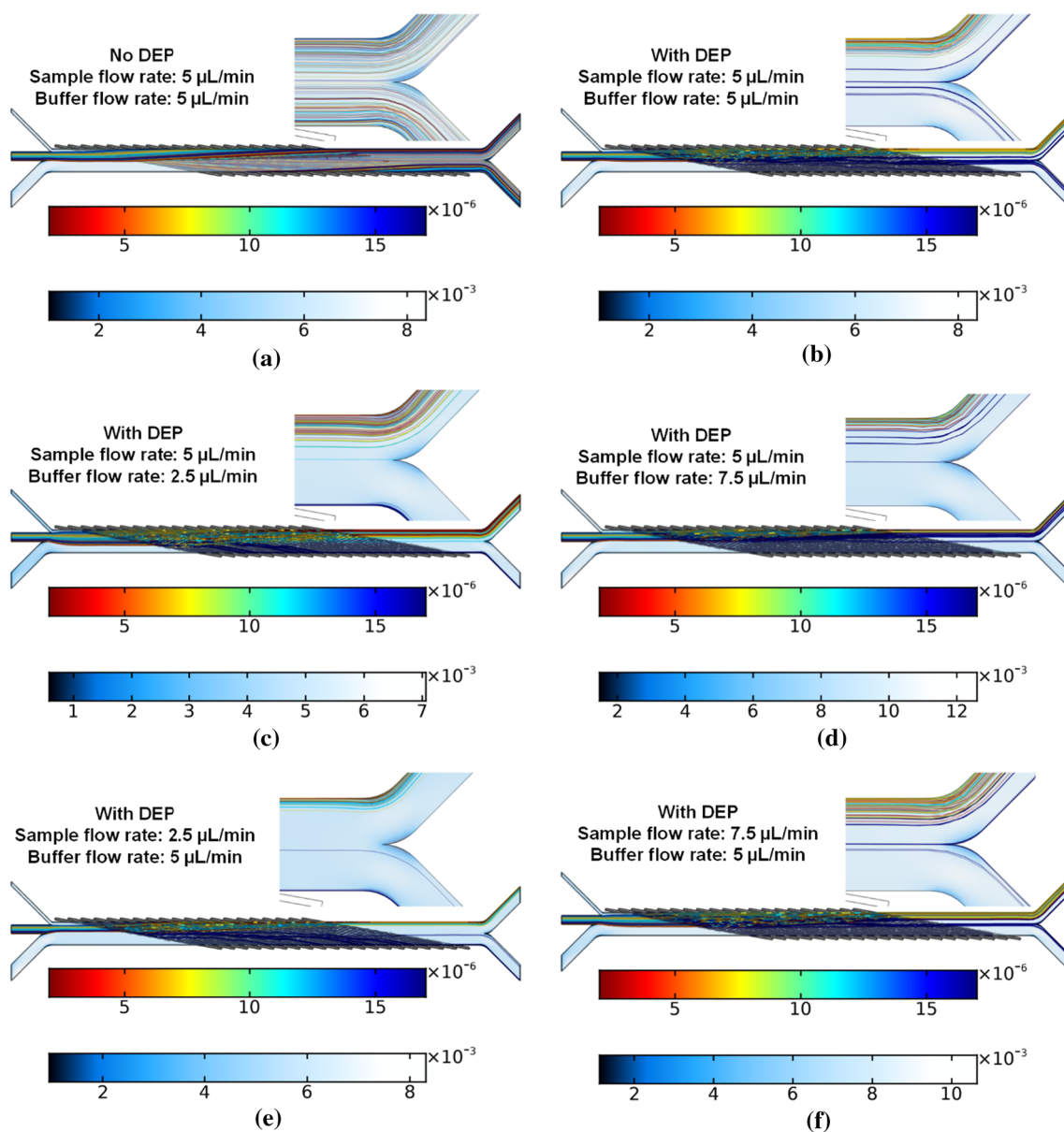


Fig. 4 Cell trajectories in the microchannel **a** without DEP and **b** with DEP manipulation at the total input flow rate of $10 \mu\text{L}/\text{min}$, and **c–f** with DEP at different cell sample and buffer flow rates

In the simulations, we also assumed that the cell samples were washed and diluted in the DEP solution before pumping into the main channel. The density and viscosity of the DEP medium in the separation region were thus almost uniform. For a given media, all cell particles have similar CM factor spectra. To achieve nDEP response onto all cells ($\text{Re}[f_{CM}] < 0$), the frequency of 5 kHz was set. Too low frequencies are not recommended, because cell survival can be drastically reduced at the very low-frequency range due to the high duration of electric impulses. Figure 2b shows the DEP factors of the cell types by Eq. (12). The DEP factor is proportional to the DEP force magnitude. In the applied

frequency, the CM factor reals for all cells are -0.5 , but DEP forces on CTCs are stronger several times than those on the other cell lines due to the size difference. As a result, most CTCs could be credibly separated from the other cells.

From the above theoretical analyses, the separation of cells is governed by the balance between DEP and hydrodynamic drag forces. The strength of the DEP force is mainly determined by the applied electric field, while the drag force is influenced by the fluid flow field in the channel. The Stokes fluid flow and electric fields and movement trajectories of cell particles in the microchannel were solved. The flowchart of the solution algorithm was

presented in our previous work [35]. After building the 3D geometrical model and creating its mesh, the boundary conditions were set. A low AC potential excitation was set on the surface of the electrodes. The inlets of the fluid flow channel were set to flow rates, the boundary condition on the channel walls was set to slip mode, and the atmospheric pressure was set at the channel outlets. The particle trajectories were computed by the combination of the DEP and Stoke's drag forces. The time-dependent solver of the particle tracing module was simulated for 10 s at a time step of 0.01 s. Tetrahedral elements were used in the simulation model mesh. More grid points were placed on the area around the electrodes due to the necessary impacts of the force fields in this region. The fine mesh was applied, consisting of 520,520 domain elements, 151,855 boundary elements, and 21,836 edge elements (see in Fig. S7). All computations were performed on an Intel Core i9-10980XE CPU @ 4.60 GHz processor with a 32 GB RAM operating system.

3 Simulation results and discussion

3.1 Simulated model validation

A similar DEP-based microfluidic design for the DEP-based manipulation of microparticles was found and verified in recent publications [13, 15]. Computational models and experimental investigations were performed to build several optimal parameters of the platform. The chip model was applied to separate 5, 10, and 15 μm polystyrene particles with a range of volumetric throughputs from 5 to 15 $\mu\text{L}/\text{min}$. The PDMS main channels of 7–14 mm length, 400–800 μm width, and 20–40 μm height were suggested. Other parameters of the width (60 μm), the spacing (20 μm), and the deflection angle (10°) of the microelectrodes were chosen. The width of the electrodes had a negligible effect on DEP forces while decreasing the electrode spacing results in higher DEP responses. However, these parameters were proposed to fit the micro-fabrication technology limitations. The microfluidic chip design was also tested for the separation of fibroblast cells. The electric frequency in kHz was selected to keep the CM factor close to -0.5. Several microfluidic chips that applied similar DEP techniques for the separation of CTCs have also been summarized in our previous study [35]. Experimental data obtained in the researches could be used to verify the simulation results. This revealed that the advanced device in the current study could also be effective for size-based cell separating and focusing applications with high aspects of recovery and purity.

The fluidic flow and the electric field distributions in modeling were considered to reveal our approach and realistic results. It is assumed that the DEP buffer solution was

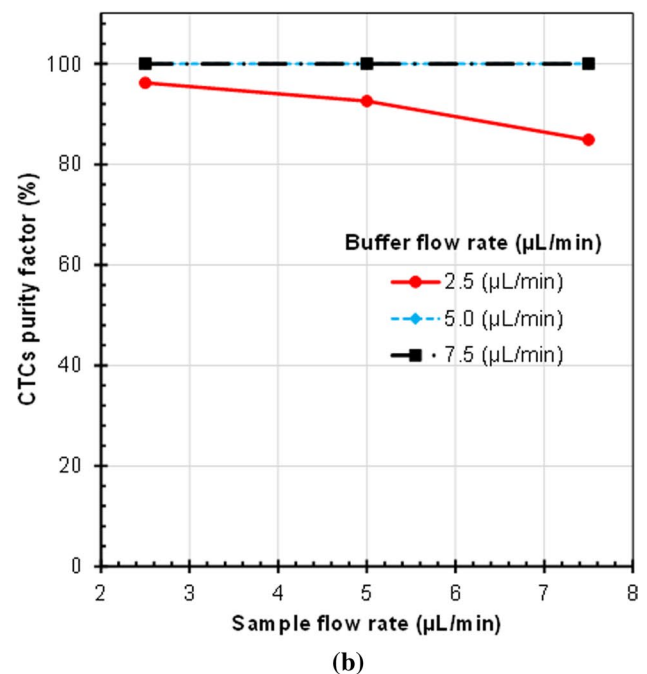
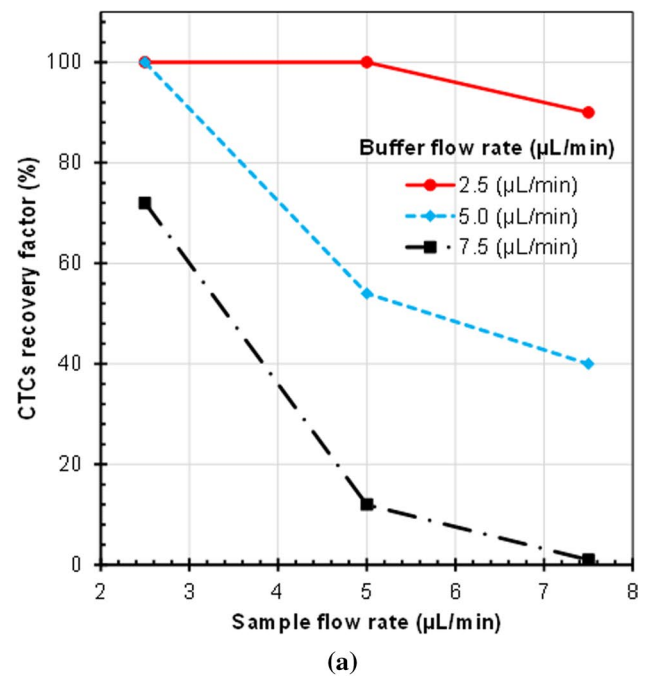


Fig. 5 CTCs recovery and purity factors with DEP manipulation at different input flow rates

injected into the channel with a total flow rate of 10 $\mu\text{L}/\text{min}$. The channel was thus filled fully with the buffer medium. In addition, the sinusoidal peak-to-peak voltage of 10 V at the frequency of 5 kHz was applied on the electrode array. Simulated velocity magnitude and electric field intensity around the separation region is expressed in Fig. 3a, b, respectively. The average velocity of the streamlines is approximately

6.0 mm/s at the cross section of the main straight channel. Besides, the velocity contours at the central flow are smaller than those of the side flows. This flow mechanism allows cell particles to be concentrated into the mid-fluidic streams of the channel as entering the DEP manipulation region. An arrangement of non-uniform electric fields on the micro-electrodes creates lateral DEP forces induced on cells. The peaks of the electric field strength are nearly 6×10^5 V/m around the edges of the electrodes. Moreover, the electric field amplitude gradually decreases with increasing the z-distance from the bottom surface to the top surface of the channel. Besides, the electric field magnitudes are quite stable in the z-range from 20 to 40 μm , with the mean value approximately 1.5×10^5 V/m. Thus, the forces acting on the nano-newton scale were exposed to have little effect on cell survival and stress.

3.2 Effect of inlet throughputs

Figure 4 exhibits the motion trajectory of cells in the channel with different inlet total flow rates. The color legend bars were used to express the cell diameters. Cells were injected into the channel through the In2 port and moved from the left to the right of the main channel. First, the tracing response at which the model had no electric excitation and the volumetric flow rate was 10 $\mu\text{L}/\text{min}$ is examined

2.5, 5.0, and 7.5 $\mu\text{L}/\text{min}$ so that the total flow rate in the main channel altered in the range from 5 to 15 $\mu\text{L}/\text{min}$. Figure 4b, d shows the cell trajectories with acting nDEP at the sample flow rate of 5 $\mu\text{L}/\text{min}$ and three different buffer flow rates. At a low buffer flow rate of 2.5 $\mu\text{L}/\text{min}$, almost all the CTCs were separated and moved to the Out2, but a little amount of smaller cells also shifted through this port (see Fig. 4c). When increasing the buffer flow equal to or higher than sample flow, all the smaller cells were focused on the top side of the Out1. However, the displacement of the CTCs also tended to shift upwards of the channel, causing some CTCs to be collected in the Out1 (see Fig. 4b). At even high flow rates, all cells, including the CTCs, were concentrated in the Out1 port (see Fig. 4d). Figure 4e, f shows the cell trajectories with acting nDEP at the buffer flow rate of 5 $\mu\text{L}/\text{min}$ and two different cell sample flow rates. Similarly, the amount of CTCs that moved upwards to the Out1 output increased with increasing the cell sample volumetric throughput.

The cell traces of the separator with different flow rates of sample and buffer in the range from 2.5 to 7.5 $\mu\text{L}/\text{min}$ were investigated. In each survey, the number of each cell type injected into the In2 port was 100. All cells were randomly released within the first second of the simulation process. After 10 s of running simulation, the cell numbers of each type collected in both output ports were determined. To evaluate the CTCs separation performance, the recovery and purity factors in the cases were defined by

$$\text{CTCs recovery factor} = \frac{\text{Number of CTCs deflected into the Out2}}{\text{Total collected CTCs in the Out1 and Out2}} \cdot 100\% \quad (14)$$

$$\text{CTCs purity factor} = \frac{\text{Number of CTCs deflected into the Out2}}{\text{Number of total cells collected in the Out2}} \cdot 100\% \quad (15)$$

and shown in Fig. 4a. Without acting electric field, the cells were only shifted by flow force to both Out1 and Out2 ports in a disorderly way. Subsequently, the movement of cells being manipulated by the lateral nDEP force was investigated on a variety of inlet flow conditions. After applying the voltage, the displacement of each cell was controlled by the net force of the DEP and the flow forces acting on it. The CTCs with the bigger size and the stronger DEP force were pushed down to the bottom side of the channel. As a result, the CTCs deflected towards the Out2 port. In comparison, the cells of WBCs, RBCs, and PLTs with smaller diameters were subjected to more drag force than DEP force. The small cells were thus repelled up to the top side of the channel and then exited in the Out1 port.

The volumetric flow rate is a highly desirable coefficient of influence on the separation of cells. Several different combinations of buffer (In1 and In3) and cell sample (In2) flow rates were explored. Their values were, respectively, set at

Figure 5a, b shows the CTCs recovery and purity factors versus the survey groups, separately. As can be seen that the CTCs recovery factor decreased as any flow rates or the total fluid stream increased. Whereas the CTCs purity factor dropped down as increasing the sample flow rate, it raised as increasing the buffer flow rate. The CTCs recovery factor achieved 100% at the sample flow rates below 5 $\mu\text{L}/\text{min}$ and the buffer flow rate of 2.5 $\mu\text{L}/\text{min}$. The recovery factor was down to about 90% when maintaining the buffer flow but increasing the sample flow up 7.5 $\mu\text{L}/\text{min}$. In these cases, the CTCs purity factors were all over 90%, but not 100%. In other cases, when the buffer stream was incremented between 5.0 and 7.5 $\mu\text{L}/\text{min}$, all the separation purity factors reached 100%. Nevertheless, all the recovery factors were less than 75%, even equal to zero when both the sample and buffer flow rates were 7.5 $\mu\text{L}/\text{min}$. Due to the demand to enhance the cancer cell isolation, the flow configurations that gave good CTCs separation factors at high sample flow

rates should be recommended. While the buffer flow rates could be maintained at a reasonable level of 2.5 $\mu\text{L}/\text{min}$.

3.3 Effect of outlet designs

In the subsequent investigation, the influence of changing the outlet design on the separation performance was mentioned. The width-based ratio between the Out1 and Out2 ports was examined. The variation was in the direction of decreasing the dimension of the Out2 while increasing the size of the Out1. This tendency corresponded to the ratio change of the inlet flow rates to move through the outlet ports. Figure 6 shows the cell trajectories with the same DEP electric field and inlet injection conditions, including the same sample flow rate of 5.0 $\mu\text{L}/\text{min}$ and the same buffer flow rate of 2.5 $\mu\text{L}/\text{min}$ at several outlets structures (Out1/Out2). As a result, the CTCs were recovered in the Out2 port with all these cases. In a case with the width of the Out1 smaller than that of the Out2, there were still some non-target cells towards the Out2, and the purity factor was thus below 100%. In the opposite cases, with the width ratio of Out1/Out2 higher than one, all the smaller cells were pushed to the Out1, and then the separation purity could achieve a high value.

The CTCs recovery and purity factors with the same DEP manipulation and the same buffer flow rate of 2.5 $\mu\text{L}/\text{min}$, but different sample flow rates from 2.5 to 7.5 $\mu\text{L}/\text{min}$ and different output designs are shown in Fig. 7a, b. The results of cell traces in all combinations are shown in Figs. S1–S5. The output width-based ratios of Out1/Out2 were set at 200/600, 300/500, 400/400, 500/300, and 600/200, respectively. In the descending trend of the Out1 size, the CTCs recovery factor dropped out, while the CTCs purity factor went up. Depending on the application, the outlet structure can be chosen to be expected efficient in terms of either recovery or purity. From these graphs, the configurations with the Out1 width located from 500 to 600 μm were preferable if the CTCs separation purity was preferred, and the recovery still achieved high performance. Both CTCs recovery and purity factors were 100% at the sample flow rate of 5.0 $\mu\text{L}/\text{min}$ and the buffer flow rate of 2.5 $\mu\text{L}/\text{min}$ (Movie 1 in the Supplementary material). Even with the Out1/Out2 ratio of 500/300, the recovery factor was still above 70%, and the purity factor was 100% at the sample flow rate of 7.5 $\mu\text{L}/\text{min}$ and the buffer flow rate of 2.5 $\mu\text{L}/\text{min}$. Hence, a duly adjusted parametric configuration that the sample flow rate is higher than the buffer flow rate; meanwhile, the more significant amount of total volumetric throughput is moved

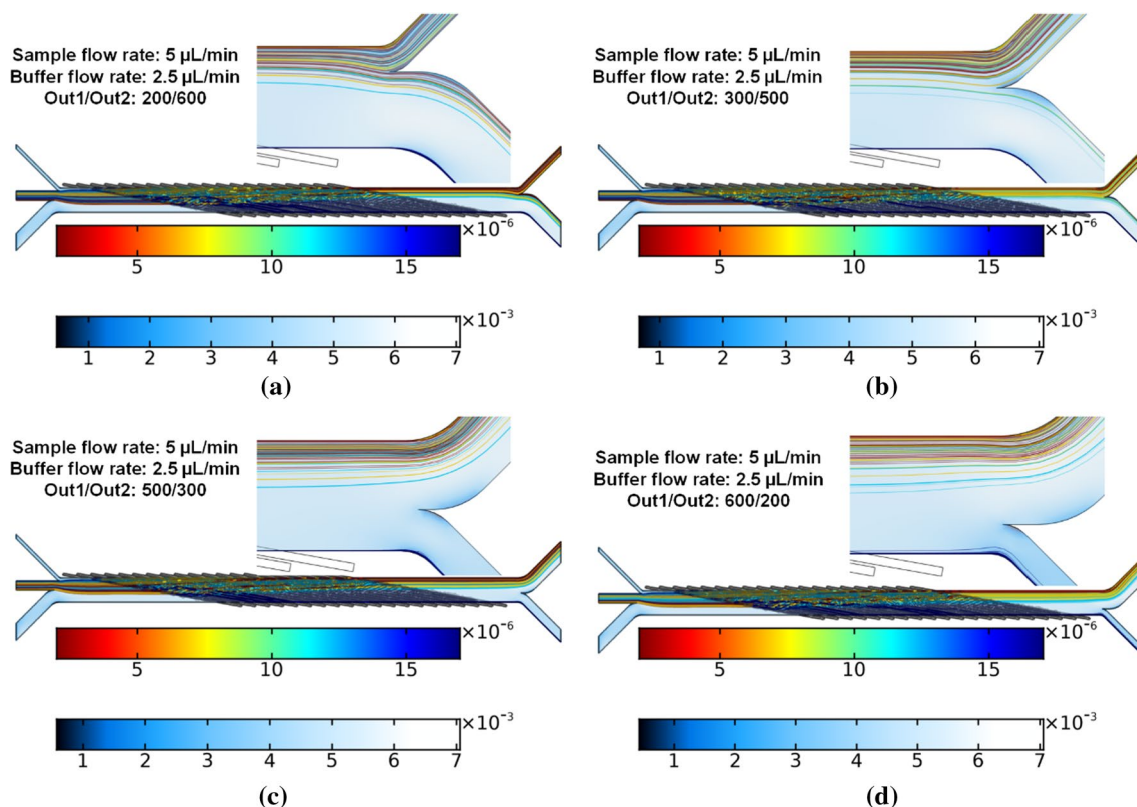


Fig. 6 Cell trajectories with being manipulated by the DEP at the sample flow rate of 5.0 $\mu\text{L}/\text{min}$, and the buffer flow rate of 2.5 $\mu\text{L}/\text{min}$; and various outlet configurations of Out1/Out2: **a** 200/600; **b** 300/500; **c** 500/300; **d** 600/200 ($\mu\text{m}/\mu\text{m}$)

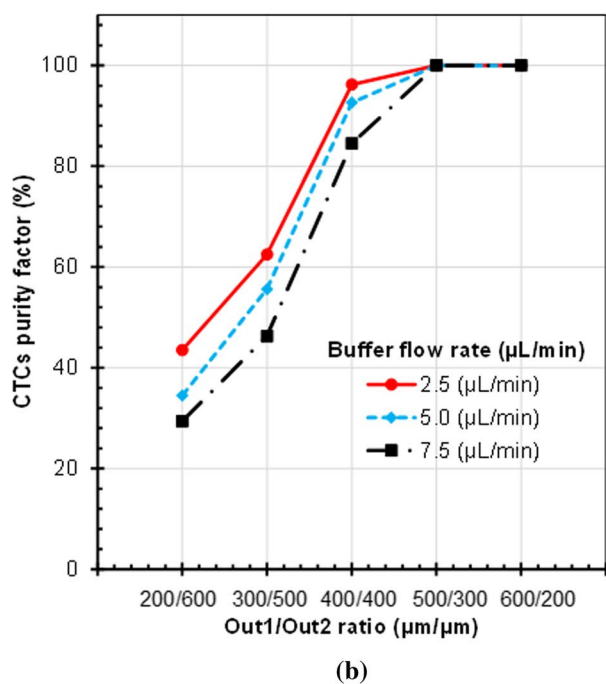
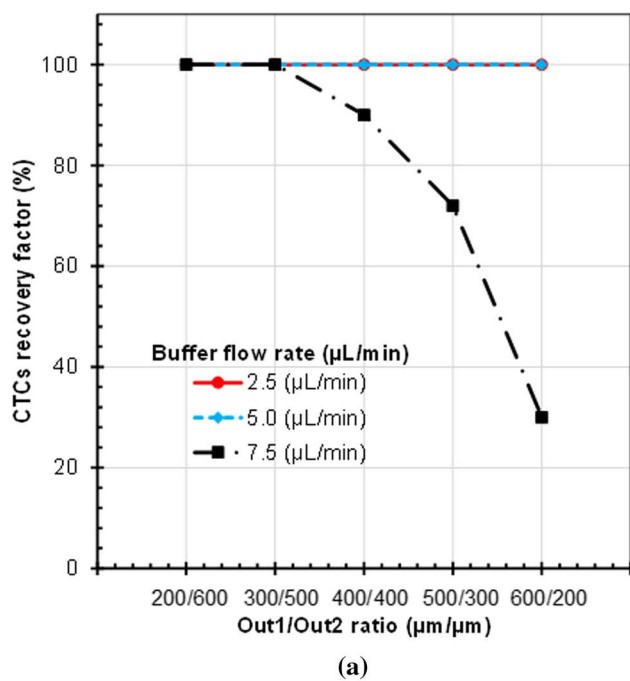


Fig. 7 CTCs recovery and purity factors at various output port designs with the same buffer flow rate of 2.5 μL/min and different sample flow rates from 2.5 to 7.5 μL/min

to the Out1 port can achieve the highest separation efficiency for the isolation of CTCs.

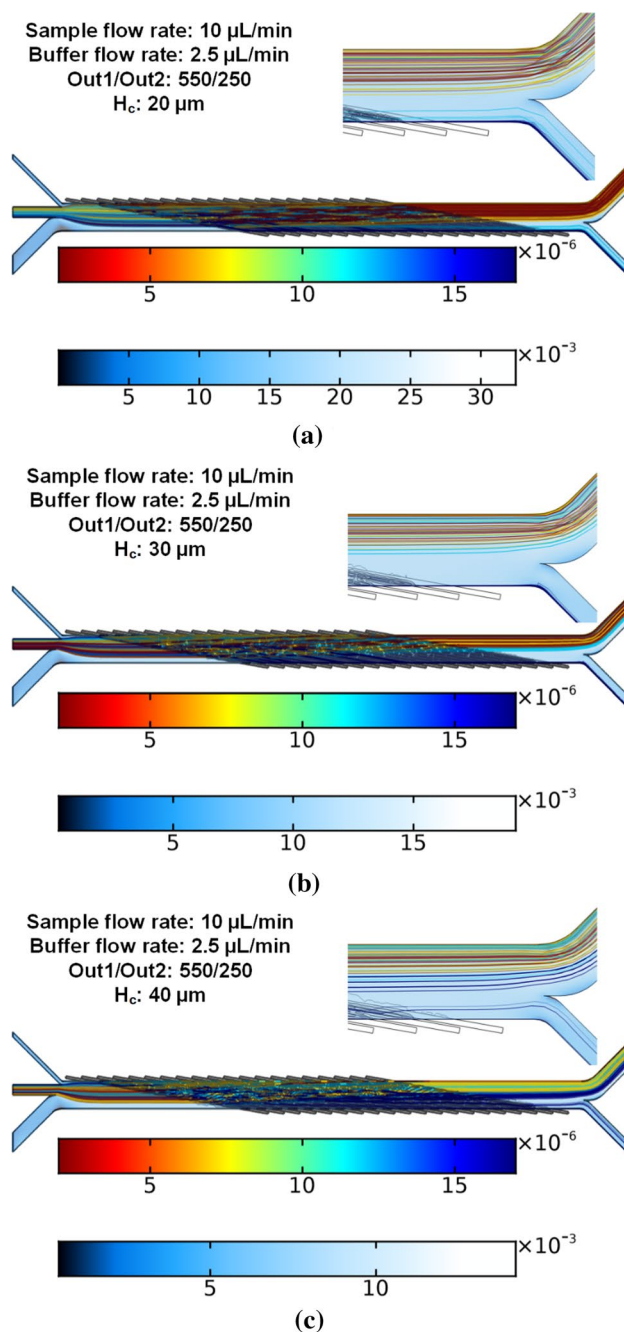


Fig. 8 Cell trajectories with being manipulated by the DEP in the three different channel height configurations from 20 to 40 μm, with the same 550/250 (μm/μm)-Out1/Out2 ratio, the same cell sample and buffer flow rates of 10 and 2.5 μL/min, respectively

3.4 Effect of channel's height

From Fig. 3b, it can be seen that the DEP force field increases as the cells move closer to the electrode surface. As the height of the channel goes down, both the effect of the electric field on cells and the flow velocity in the separation region grow up. In the subsequent survey, the influence

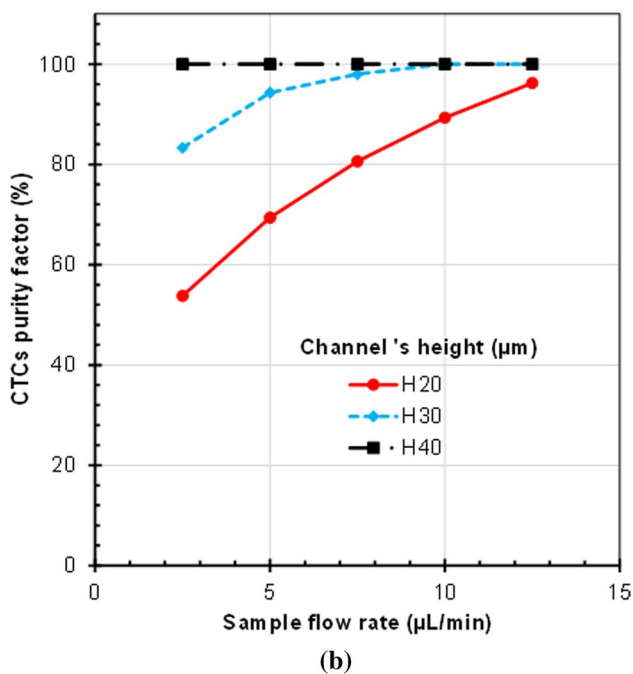
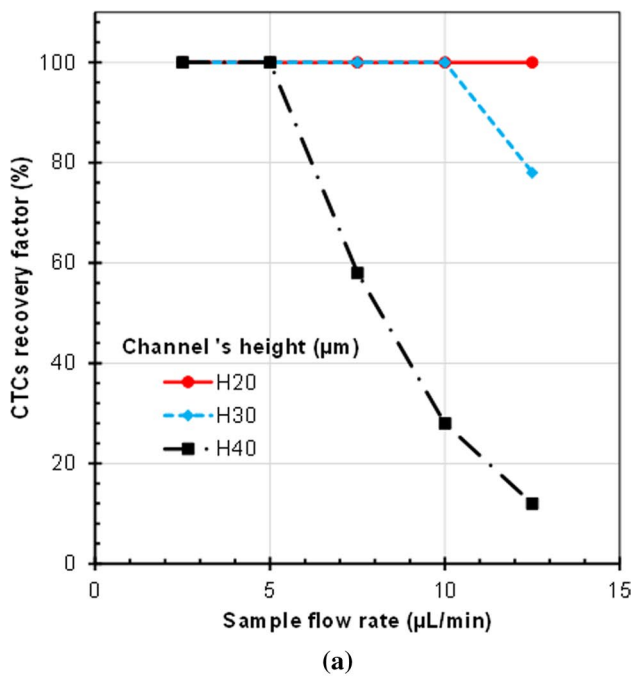


Fig. 9 CTCs recovery and purity factors at various channel height configurations ($H=20, 30, 40 \mu\text{m}$) with the same buffer flow rate of $2.5 \mu\text{L}/\text{min}$ and different sample flow rates from 2.5 to $12.5 \mu\text{L}/\text{min}$

of the channel's height was mentioned. Three microchannel configurations with the same Out1/Out2 ratio of $550/250$ and different heights from 20 to $40 \mu\text{m}$, were considered. These channel height dimensions are still larger than the diameters of all cell types. The investigations were performed at the same buffer flow rate of $2.5 \mu\text{L}/\text{min}$ with several sample flow rates ranging from 2.5 to $12.5 \mu\text{L}/\text{min}$. Figure 8a–c shows

the cell trajectory plots at the same cell sample flow rate of $10 \mu\text{L}/\text{min}$ for the three different channel height designs. More detailed information for all the cases were given in Fig. S6. The CTCs recovery and purity factors are calculated and shown in Fig. 9. With the low channel height of $20 \mu\text{m}$, DEP effects strongly acted on all cells. This results in not only CTCs but also some other blood cells (usually WBCs) being separated into the Out2 exit. Thus, the CTCs recovery factors are high, but the CTCs purity factors are lower than 100% . On the contrary, the CTCs recovery factors decrease, but the CTCs separation purity factors are high for the channel height size of $40 \mu\text{m}$. The microchannel configuration with the height of $30 \mu\text{m}$ is suggested to maintain good separation performances. The results indicated that the proposed design achieved both the CTCs recovery and purity factors of 100% with the cell sample flow rate of $10 \mu\text{L}/\text{min}$ (see Fig. 8b). This property creates an excellent possibility for size-based cell separation applications (such as cancer cell enrichment from other blood cells).

4 Conclusions

A continuous-flow and DEP-based microfluidic chip was successfully developed and validated using the 3D computational model to separate lung CTCs from other blood cells, including WBCs, RBCs, and PLTs. Various optimal parameters of the microfluidic channel, the electrode array, the length of the DEP region, and the applied electric field were chosen by the suggestions in the literature. In this paper, the volumetric throughputs into the inlet and outlet ports were examined to improve the recovery and purity factors for the isolation of CTCs towards the below side outlet of the channel. With the assumptions of fixed shape and size of cells, the microchannel configuration with the dimensions of $30 \mu\text{m}$ -height, $550 \mu\text{m}$ -width for Out1 and $250 \mu\text{m}$ -width for Out2 could achieve the performance factors of 100% when the cell sample flow rate is about $10 \mu\text{L}/\text{min}$, and the buffer flow rate is $2.5 \mu\text{L}/\text{min}$. Though, the throughput of this microfluidic flow-separating device is still limited to processing an actual blood sample. The multi-parallel channel structures may be considered to improve the robustness of its operation. The findings and simulation results of this work can help determine the optimal parameters for the development of portable DEP-based platforms with a higher sample throughput for CTCs detection as well as metastatic cancer diagnosis and prognosis. Changing the cell size range, verifying the CTCs separation efficiency from the peripheral blood sample, and enhancing the cell sample throughput could be explored in the proceeding works.

Supplementary Information The online version contains supplementary material available at <https://doi.org/10.1007/s13367-022-00039-6>.

Acknowledgements This work was supported by The Phenikaa University Foundation for Science and Technology Development. The authors would also like to thank Vietnam National University, Hanoi for supporting some computational tools.

Declarations

Conflict of interest The authors have declared no conflict of interest.

References

1. Aghaamoo M, Aghilinejad A, Chen X (2017) Numerical study of insulator-based dielectrophoresis method for circulating tumor cell separation. In: *Microfluidics, BioMEMS, and Medical Microsystems XV*. pp 100611A–11
2. Alam MK, Koomson E, Zou H, Yi C, Li CW, Xu T, Yang M (2018) Recent advances in microfluidic technology for manipulation and analysis of biological cells (2007–2017). *Anal Chim Acta* 1044:29–65. <https://doi.org/10.1016/j.aca.2018.06.054>
3. Alazzam A, Mathew B, Alhamadi F (2017) Novel microfluidic device for the continuous separation of cancer cells using dielectrophoresis. *J Sep Sci* 40:1193–1200. <https://doi.org/10.1002/jssc.201601061>
4. Ali H, Park CW (2016) Numerical study on the complete blood cell sorting using particle tracing and dielectrophoresis in a microfluidic device. *Korea Aust Rheol J* 28:327–339. <https://doi.org/10.1007/s13367-016-0033-4>
5. Aljaghtham MS, Liu ZL, Guo JJ, He J, Celik E (2019) Numerical simulations of cell flow and trapping within microfluidic channels for stiffness based cell isolation. *J Biomech* 85:43–49. <https://doi.org/10.1016/j.jbiomech.2019.01.010>
6. Alshareef M, Metrakos N, Juarez Perez E, Azer F, Yang F, Yang X, Wang G (2013) Separation of tumor cells with dielectrophoresis-based microfluidic chip. *Biomicrofluidics* 7:1–12. <https://doi.org/10.1063/1.4774312>
7. Amstad E, Chen X, Eggersdorfer M, Cohen N, Kodger TE, Ren CL, Weitz DA (2017) Parallelization of microfluidic flow-focusing devices. *Phys Rev E* 95:1–6. <https://doi.org/10.1103/PhysRevE.95.043105>
8. Balakrishnan SG, Ahmad MR, Koloro SSR, Petrù M (2021) Separation of ctDNA by superparamagnetic bead particles in microfluidic platform for early cancer detection. *J Adv Res*. <https://doi.org/10.1016/j.jare.2021.03.001>
9. Chen J, Li J, Sun Y (2012) Microfluidic approaches for cancer cell detection, characterization, and separation. *Lab Chip* 12:1753–1767. <https://doi.org/10.1039/c2lc21273k>
10. Chen Y, Li P, Huang PH, Xie Y, Mai JD, Wang L, Nguyen NT, Huang TJ (2014) Rare cell isolation and analysis in microfluidics. *Lab Chip* 14:626–645. <https://doi.org/10.1039/c3lc90136j>
11. Choi S, Lee H, Lee S, Park I, Kim YS, Key J, Lee SY, Yang S, Lee SW (2020) A novel automatic segmentation and tracking method to measure cellular dielectrophoretic mobility from individual cell trajectories for high throughput assay. *Comput Methods Programs Biomed* 195:105662. <https://doi.org/10.1016/j.cmpb.2020.105662>
12. Dabighi A, Toghraie D (2020) A new microfluidic device for separating circulating tumor cells based on their physical properties by using electrophoresis and dielectrophoresis forces within an electrical field. *Comput Methods Programs Biomed* 185:105147. <https://doi.org/10.1016/j.cmpb.2019.105147>
13. Dalili A, Montazerian H, Sakthivel K, Tasnim N, Hoorfar M (2021) Dielectrophoretic manipulation of particles on a microfluidics platform with planar tilted electrodes. *Sensors Actuators, B Chem* 329:129204. <https://doi.org/10.1016/j.snb.2020.129204>
14. Dalili A, Samiei E, Hoorfar M (2019) A review of sorting, separation and isolation of cells and microbeads for biomedical applications: microfluidic approaches. *Analyst* 144:87–113. <https://doi.org/10.1039/c8an01061g>
15. Dalili A, Taatizadeh E, Tahmooressi H, Tasnim N, Rellstabs-Sánchez PI, Shaunessy M, Najjaran H, Hoorfar M (2020) Parametric study on the geometrical parameters of a lab-on-a-chip platform with tilted planar electrodes for continuous dielectrophoretic manipulation of microparticles. *Sci Rep* 10:1–11. <https://doi.org/10.1038/s41598-020-68699-4>
16. Farahinia A, Zhang WJ, Badaea I (2021) Novel microfluidic approaches to circulating tumor cell separation and sorting of blood cells: a review. *J Sci Adv Mater Devices* 6:303–320. <https://doi.org/10.1016/j.jsamd.2021.03.005>
17. Ghita M, Copot D, Ionescu CM (2021) Lung cancer dynamics using fractional order impedance modeling on a mimicked lung tumor setup. *J Adv Res* 32:61–71. <https://doi.org/10.1016/j.jare.2020.12.016>
18. Gupta T, Ghosh R, Ganguly R (2018) Acoustophoretic separation of infected erythrocytes from blood plasma in a microfluidic platform using biofunctionalized, matched-impedance layers. *Int J Numer Method Biomed Eng*. <https://doi.org/10.1002/cnm.2943>
19. Hajari M, Ebadi A, FarshchiHeydari MJ, Fathipour M, Soltani M (2020) Dielectrophoresis-based microfluidic platform to sort micro-particles in continuous flow. *Microsyst Technol* 26:751–763. <https://doi.org/10.1007/s00542-019-04629-3>
20. Hajba L, Guttman A (2014) Circulating tumor-cell detection and capture using microfluidic devices. *TrAC - Trends Anal Chem* 59:9–16. <https://doi.org/10.1016/j.trac.2014.02.017>
21. Han KH, Han SI, Frazier AB (2009) Lateral displacement as a function of particle size using a piecewise curved planar interdigitated electrode array. *Lab Chip* 9:2958–2964. <https://doi.org/10.1039/b909753h>
22. Hao S, Wan Y, Xia Y, Zou X, Zheng S (2018) Size-based separation methods of circulating tumor cells. *Adv Drug Deliv Rev* 125:3–20. <https://doi.org/10.1016/j.addr.2018.01.002>
23. Jen CP, Chen TW (2009) Selective trapping of live and dead mammalian cells using insulator-based dielectrophoresis within open-top microstructures. *Biomed Microdevices* 11:597–607. <https://doi.org/10.1007/s10544-008-9269-1>
24. Kazemi B, Darabi J (2018) Numerical simulation of dielectrophoretic particle separation using slanted electrodes. *Phys Fluids* 30:102003. <https://doi.org/10.1063/1.5047153>
25. Kenig EY, Su Y, Lautenschleger A, Chasanis P, Grünwald M (2013) Micro-separation of fluid systems: a state-of-the-art review. *Sep Purif Technol* 120:245–264. <https://doi.org/10.1016/j.seppur.2013.09.028>
26. Kinnunen M, Kauppila A, Karmenyan A, Myllylä R (2011) Effect of the size and shape of a red blood cell on elastic light scattering properties at the single-cell level. *Biomed Opt Express* 2:1803. <https://doi.org/10.1364/boe.2.001803>
27. Li M, Anand RK (2017) High-throughput selective capture of single circulating tumor cells by dielectrophoresis at a wireless electrode array. *J Am Chem Soc* 139:8950–8959. <https://doi.org/10.1021/jacs.7b03288>
28. Li M, Li WH, Zhang J, Alici G, Wen W (2014) A review of micro-fabrication techniques and dielectrophoretic microdevices for particle manipulation and separation. *J Phys D Appl Phys* 47:063001. <https://doi.org/10.1088/0022-3727/47/6/063001>
29. Liang W, Liu J, Yang X, Zhang Q, Yang W, Zhang H, Liu L (2020) Microfluidic-based cancer cell separation using active and

- passive mechanisms. *Microfluid Nanofluidics*. <https://doi.org/10.1007/s10404-020-2331-x>
30. Lozar T, Gersak K, Cemazar M, Kuhar CG, Jesenko T (2019) The biology and clinical potential of circulating tumor cells. *Radiol Oncol* 53:131–147. <https://doi.org/10.2478/raon-2019-0024>
 31. Marchalot J, Chateaux JF, Faivre M, Mertani HC, Ferrigno R, Deman AL (2015) Dielectrophoretic capture of low abundance cell population using thick electrodes. *Biomicrofluidics* 9:054104. <https://doi.org/10.1063/1.4928703>
 32. Mohamed Zackria MZA, Tirth V, Yousuff CM, Shukla NK, Islam S, Irshad K, Aarif KOM (2020) Simulation Guided Microfluidic Design for Multitarget Separation Using Dielectrophoretic Principle. *Biochip J* 14:390–404. <https://doi.org/10.1007/s13206-020-4406-x>
 33. Nguyen NV, Jen CP (2018) Impedance detection integrated with dielectrophoresis enrichment platform for lung circulating tumor cells in a micro fluidic channel. *Biosens Bioelectron* 121:10–18. <https://doi.org/10.1016/j.bios.2018.08.059>
 34. Nguyen NV, Jen CP (2019) Selective detection of human lung adenocarcinoma cells based on the aptamer-conjugated self-assembled monolayer of gold nanoparticles. *Micromachines* 10:195. <https://doi.org/10.3390/mi10030195>
 35. Nguyen NV, Le Manh T, Nguyen TS, Le VT, Van Hieu N (2021) Applied electric field analysis and numerical investigations of the continuous cell separation in a dielectrophoresis-based microfluidic channel. *J Sci Adv Mater Devices* 6:11–18. <https://doi.org/10.1016/j.jsamd.2020.11.002>
 36. Nguyen NV, Yeh JH, Jen CP (2018) A handheld electronics module for dielectrophoretic impedance measurement of cancerous cells in the microchip. *Biochip J* 12:208–215. <https://doi.org/10.1007/s13205-015-9306-8>
 37. Okano H, Konishi T, Suzuki T, Suzuki T, Ariyasu S, Aoki S, Abe R, Hayase M (2015) Enrichment of circulating tumor cells in tumor-bearing mouse blood by a deterministic lateral displacement microfluidic device. *Biomed Microdevices* 17:1–11. <https://doi.org/10.1007/s10544-015-9964-7>
 38. Ou X, Chen P, Huang X, Li S, Liu BF (2020) Microfluidic chip electrophoresis for biochemical analysis. *J Sep Sci* 43:258–270. <https://doi.org/10.1002/jssc.201900758>
 39. Panklang N, Techaumnat B, Wisitorsaat A (2020) Analysis of the equivalent dipole moment of red blood cell by using the boundary element method. *Eng Anal Bound Elem* 112:68–76. <https://doi.org/10.1016/j.enganabound.2019.12.002>
 40. Panwar N, Song P, Tjin SC, Yong K-T (2018) Sheath-assisted hydrodynamic particle focusing in higher Reynolds number flows. *J Micromech Microeng* 28:105018
 41. Piacentini N, Mernier G, Tornay R, Renaud P (2011) Separation of platelets from other blood cells in continuous-flow by dielectrophoresis field-flow-fractionation. *Biomicrofluidics* 5:034122. <https://doi.org/10.1063/1.3640045>
 42. Qian C, Huang H, Chen L, Li X, Ge Z, Chen T, Yang Z, Sun L (2014) Dielectrophoresis for bioparticle manipulation. *Int J Mol Sci* 15:18281–18309. <https://doi.org/10.3390/ijms151018281>
 43. Sharma S, Zhuang R, Long M, Pavlovic M, Kang Y, Ilyas A, Asghar W (2018) Circulating tumor cell isolation, culture, and downstream molecular analysis. *Biotechnol Adv* 36:1063–1078
 44. Song H, Rosano JM, Wang Y, Garson CJ, Prabhakarapandian B, Pant K, Klarmann GJ, Perantoni A, Alvarez LM, Lai E (2015) Continuous-flow sorting of stem cells and differentiation products based on dielectrophoresis. *Lab Chip* 15:1320–1328. <https://doi.org/10.1039/c4lc01253d>
 45. Sun L, Yang W, Cai S, Chen Y, Chu H, Yu H, Wang Y, Liu L (2020) Recent advances in microfluidic technologies for separation of biological cells. *Biomed Microdevices*. <https://doi.org/10.1007/s10544-020-00510-7>
 46. Sung H, Ferlay J, Siegel RL, Laversanne M, Soerjomataram I, Jemal A, Bray F (2021) Global Cancer Statistics 2020: GLOBOCAN estimates of incidence and mortality worldwide for 36 cancers in 185 countries. *CA Cancer J Clin* 71:209–249. <https://doi.org/10.3322/caac.21660>
 47. Turcan I, Olariu MA (2020) Dielectrophoretic manipulation of cancer cells and their electrical characterization. *ACS Comb Sci* 22:554–578. <https://doi.org/10.1021/acscombsci.0c00109>
 48. Yin J, Deng J, Du C, Zhang W, Jiang X (2019) Microfluidics-based approaches for separation and analysis of circulating tumor cells. *TrAC - Trends Anal Chem* 117:84–100. <https://doi.org/10.1016/j.trac.2019.07.018>
 49. Zhang X, Xu X, Ren Y, Yan Y, Wu A (2021) Numerical simulation of circulating tumor cell separation in a dielectrophoresis based Y-Y shaped microfluidic device. *Sep Purif Technol* 255:117343. <https://doi.org/10.1016/j.seppur.2020.117343>
 50. Zhou J, Kulasinghe A, Bogseth A, O'Byrne K, Punyadeera C, Papautsky I (2019) Isolation of circulating tumor cells in non-small-cell-lung-cancer patients using a multi-flow microfluidic channel. *Microsystems Nanoeng* 5:8. <https://doi.org/10.1038/s41378-019-0045-6>
 51. Zhu Z, Wu D, Li S, Han Y, Xiang N, Wang C, Ni Z (2021) A polymer-film inertial microfluidic sorter fabricated by jigsaw puzzle method for precise size-based cell separation. *Anal Chim Acta* 1143:306–314. <https://doi.org/10.1016/j.aca.2020.11.001>

Publisher's Note Springer Nature remains neutral with regard to jurisdictional claims in published maps and institutional affiliations.

Springer Nature or its licensor holds exclusive rights to this article under a publishing agreement with the author(s) or other rightsholder(s); author self-archiving of the accepted manuscript version of this article is solely governed by the terms of such publishing agreement and applicable law.

Authors and Affiliations

Ngoc-Viet Nguyen^{1,2}  · Hoang Van Manh³ · Nguyen Van Hieu^{1,2}

¹ Faculty of Electrical and Electronic Engineering, Phenikaa University, Hanoi 12116, Vietnam

² Phenikaa Research and Technology Institute (PRATI), A&A Green Phoenix Group JSC, No. 167 Hoang Ngan, Trung Hoa, Cau Giay, Hanoi 11313, Vietnam

³ Faculty of Engineering Mechanics and Automation, VNU-University of Engineering and Technology, Hanoi 10000, Vietnam